REVIEWS in
MINERALOGY &
GEOCHEMISTRY
Volume 42

MOLECULAR MODELING THEORY:
APPLICATIONS IN THE GEOSCIENCES

R. T. CYGAN, J. D. KUBICKI, EDITORS

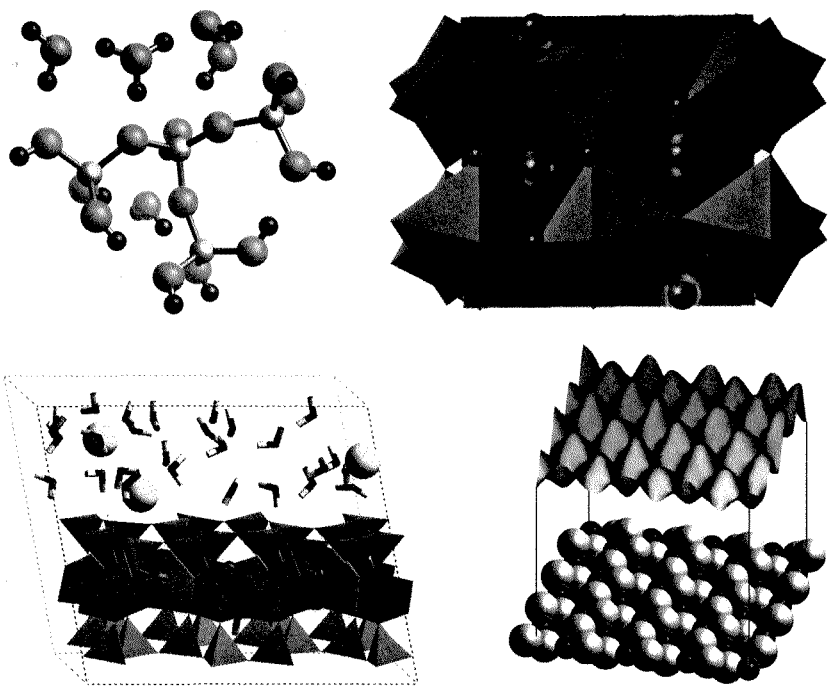

GEOCHEMICAL SOCIETY
Jodi J. Rosso, *Series Editor*
MINERALOGICAL SOCIETY OF AMERICA
Paul H. Ribbe, *Series Editor*
2001 *ISSN 1529-6466*

6 **Molecular Models of Surface Relaxation, Hydroxylation, and Surface Charging at Oxide-Water Interfaces**

James R. Rustad

6

Molecular Models of Surface Relaxation, Hydroxylation, and Surface Charging at Oxide-Water Interfaces

James R. Rustad

W.R. Wiley Environmental Molecular Sciences Laboratory
Pacific Northwest National Laboratory
P.O. Box 999, MSIN K8-96
Richland, Washington, 99352, U.S.A.

INTRODUCTION

Increasingly sophisticated experimental techniques are resolving detailed aspects of the surface chemistry of oxide and silicate materials. Structural characterization can now be carried out on remarkably complex systems (Brown et al. 1999). Recent examples include the distribution of iron in dioctahedral smectites (Manceau et al. 2000), the arrangements of protons on the hematite (012) surface (Henderson et al. 1998), the relaxation of iron atoms at the surface of hematite (001) (Thevuthasan et al. 1999), the arrangements of defects in the γ-Fe_2O_3 corrosion film formed on metallic iron (Ryan et al. 2000), the existence of two terminations of magnetite (001) (Stanka et al. 2000), and the structure of the Cr(III) passivation layer formed on magnetite as a result of magnetite-induced reduction of aqueous Cr(VI) (Peterson et al. 1997). Mesoscale structural studies include measurement and quantification of surface morphology using scanning probe and x-ray scattering methods (Eggleston and Stumm 1993; Weidler et al. 1998a,b). Similar developments are taking place in the measurement of reaction energetics and kinetics, such as temperature programmed desorption studies of the binding energies of water molecules on oxide and sulfide surfaces (Bebie et al. 1998; Stirniman et al. 1998; Henderson et al. 1998; Peden et al. 1999), the binding of phosphate on hematite (Nooney et al. 1996), and the measurement of surface energies through high resolution calorimetric investigations (McHale et al. 1997; Laberty and Navrotsky 1997).

As these developments allow investigation of surfaces on increasingly small scales, it becomes more difficult to collect these experiments together into a coherent model, to link them with experiments on macroscopic systems in the laboratory (Sposito 1999), and bring the results to bear on complex, multicomponent natural systems. For example, measurement of the amount of surface relaxation taking place on vacuum-terminated hematite (001) gives some insight into the chemical characteristics of the energies and forces associated with the Fe-O bond. This information is highly specific to the particular structural environment in which this bond is formed. It is difficult, for instance, to draw any conclusions about the arrangements of protons on hematite (012) from knowledge about the shortening of the surface Fe-O bond on cleavage of vacuum-terminated hematite (001), even though the latter observation in principle forms an important constraint on the former. Furthermore, knowledge of the proton distribution on monolayer-hydroxylated hematite (012) is obviously valuable in understanding its surface charging behavior, yet one cannot directly use the proton speciation information determined in (Henderson et al. 1998) to predict the surface charge as a function of pH. Other questions of this nature are: Is the high threshold pressure for hydroxylation of corundum relative to hematite (Liu et al. 1998) related in any way to the lower acidity of $Al(H_2O)_6^{3+}$ relative to $Fe(H_2O)_6^{3+}$ in aqueous solution? How do the observations of the structural characteristics of reduced nontronites worked out by Manceau et al. (2000)

1529-6466/00/0042-0006$05.00

affect the interpretation of the XPS experiments of Ilton et al. (1997) on the oxidation of biotite by chromate?

Computer simulation can play an important role in answering these types of questions, particularly in forming the important connection between high-vacuum surface science techniques and sorption in solvated systems. Computer models can be used to calculate the amount of relaxation on vacuum-terminated hematite (001) (Wasserman et al. 1997; Wang et al. 1998), the difference in acidity between $Fe(H_2O)_6^{3+}$ and $Al(H_2O)_6^{3+}$ (Rustad et al. 1999a), and potentially, the energies of the various proton and iron(III) distributions proposed for reduced nontronite. Then, if these calculations agree with experimental observations, the same models can, at least in principle, be used to simulate more complex processes, such as the distribution of protons on hematite (012), the hydroxylation pressure of hematite and corundum, and the oxidation of biotite by chromate. In practice, computational power limits (possibly severely) the length and time scales available to simulations (see Harding 1997 for an excellent review). However, there is little doubt that simulation is the only realistic path toward answering such questions, and it is playing an increasingly important part in the unification and correlation of the results of these complex experiments as well as providing a major avenue between these molecular scale experiments and thermodynamics (Blonski and Garofalini 1993; McCarthy et al. 1996; McCoy and Lafemina 1997; Gibson and LaFemina 1997; Felmy and Rustad 1998; Hartzell et al. 1998; Henderson et al. 1998; Rustad et al. 1999b; Brown et al. 1999; Halley et al. 1999; de Leeuw et al. 1996, 1998, 2000; Brown et al. 2000; Rustad and Dixon 2001).

SCOPE

First it should be pointed out that this review is focused primarily on examples drawn from our own research group, and does not constitute a comprehensive review of the literature. Good introductions to molecular dynamics methods abound (Frenkel and Smit 1996; Allen and Tildesley 1989). An exceptionally clear discussion can be found in Bennett (1975). Reviews of general aspects of computational modeling of surfaces and interfaces with a geochemical emphasis are provided in Gibson and LaFemina (1997) or Rustad and Dixon (1998). This review is meant to complement those articles by considering some dominant issues arising in our research on solvated/hydroxylated oxide surfaces. The discussion of these specific issues likely will be useful to those designing similar research programs focused on inorganic aqueous interfacial chemistry.

Molecular simulation has a broad scope, ranging from calculation of the trajectory of a 100 atom system for a few picoseconds using direct dynamics with *ab initio* forces (Car and Parrinello 1985), to systems with thousands of atoms simulated for a few nanoseconds (deLeuuw et al. 1996, 1998; Wasserman et al. 1997; Jones et al. 2000), to large-scale molecular dynamics studies using millions of atoms (Vaidehi and Goddard 2000; Campbell et al. 1999) to kinetic Monte Carlo (McCoy and LaFemina 1997) and dissipative particle dynamics simulation of crystal growth over length scales of microns (Dzwinel and Yuen 2000; see Yuen and Rustad 1999 for additional references). All of these categories are concerned with simulation, meaning that they are essentially numerical experiments, subject to statistical uncertainties, careful control of experimental conditions such as pressure/stress, temperature, and composition, and concerns about reproducibility and independence of initial conditions. In this review, we focus on the thousand atom/nanosecond timescale range. For convenience, we refer to these types of simulations as "classical" MD. "Parameterized" MD is actually a better term; such simulations can treat the dynamics quantum mechanically if so desired (Strauss and Voth 1993).

One reason for this focus is that there have been very few simulation studies on systems of geochemical relevance outside this scale. Partly, this lack of studies results from the fact that the thousand atom nanosecond timescale studies on interfacial systems are still in infancy themselves. In some sense, this ground must be understood thoroughly before studies at other scales can be justified/directed. For example, a picosecond direct dynamics simulation of a model mineral-water surface is not sufficient to define any interesting energetic quantities, or even structural averages, that can be regarded as independent of the initial conditions of the numerical experiment. These initial conditions must therefore be chosen carefully, with some knowledge of the approximate behavior of the system. The shorter the timescale of the simulation, the greater the knowledge required to define the initial conditions. At the other extreme are kinetic Monte Carlo studies in which molecular degrees of freedom are eliminated and the simulation parameters are chosen to represent the frequencies of "fundamental events" such as the probabilities of attachment of an atom at various surface sites presumed to exist at the interface. At both ends of this spectrum, the influence of the practitioner on the simulation results is high: at the lower end, through the choice of initial conditions; on the upper end, through the choice of event frequency parameters. Both of these techniques can be very effective but both benefit from the information generated at the classical MD scale to reduce the arbitrary aspects of the practioner influence. As computers evolve, these considerations will be modified; one can imagine the Car-Parrinello methods at some point will completely encompass the parameterized MD studies at the length and time scales under consideration here, particularly as pseudopotentials are treated using more general methods (Bloechl 1994; Vanderbilt 1990). But parameterized methods have survived the decade of vector to parallel revolution without being pushed into irrelevantly large system sizes. With the increasing recognition of role nanoscale heterogeneity in controlling structure-reactivity relationships (Weidler 1998a,b; Zhang et al. 1999), parameterized methods will likely survive through the next decade as well.

As a first step, the simulation of a mineral-aqueous interface requires treatment of the issue of surface hydroxylation, which is fundamentally tied to the dissociation of water and the energetics of acid-base reactions on mineral surfaces (Blesa et al. 2000). Even just setting the problem up requires some knowledge of the protonation states of the oxide ions at the surface; are they aquo, hydroxo, or oxo functional groups? If one cannot describe the processes behind Figure 1, it is not possible to go further. This description is

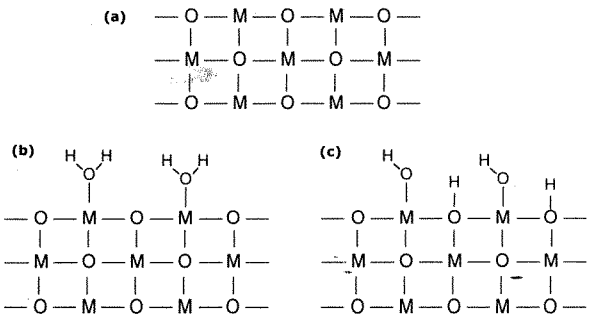

Figure 1. Schematic illustration of terminology for oxide surfaces used in this paper (a) vacuum-terminated surface, (b) hydrated surface with no dissociation of water, (c) hydroxylated surface with adsorbed water fully dissociated.

the major bottleneck in applying molecular dynamics methods to the aqueous mineral interface.

There are potentially many ways to treat this problem using analytical force fields. The simplest is to leave the surface speciation issue to empirical methods. There are empirical estimates of surface pK_as even for multisite models of surface protonation (Hiemstra et al. 1996). One could use these methods to estimate a population of surface sites, then use a well-understood water model, such as SPC/E or TIP4P to solvate this surface. The advantage of this approach is that we can effectively bypass the problem of surface hydroxylation and focus on larger-scale problems, such as the structure of the electric double layer using a water model known to give good transport and dielectric properties and which already has been used in the parameterization of alkali and alkaline earth cations and several anions. The main argument against this approach is that while the empirical methods can be effective in representing or fitting macroscopic phenomena such as surface charging, they may have little basis in molecular reality. It would be dangerous to use "fitted" molecular species from a thermodynamic analysis as a literal representation of molecular level structure. Given that the primary influence on the electric double layer will come from the speciation of the proton, the most important potential-determining ion, conclusions drawn about the interface without a firm picture of the solid side of the hydroxylated interface would be of limited defensibility.

Halley et al. (1993) following Stillinger and David (1980) have attempted to treat the water dissociation problem explicitly using the potential functions. In this approach, the O-H interaction is treated like any other interaction, with a finite range and a meaningful well depth. For example, a collection of O^{2-} and H^+ ions, if placed at randomly in a computational cell, should give rise to something like water. The water molecule forms as a result of the potential and is not put in explicitly a priori. The rest of this review is a discussion of the results of applying the Stillinger-David water model to problems related to hydroxylated mineral surface structures and energies.

THE STILLINGER-DAVID WATER MODEL

Stillinger and David (1980) developed an ionic model for water that was capable of dissociation into ions. In addition to being the only dissociating parameterized model for water, this was also one of the first polarizable water models. The explicit incorporation of oxygen polarizability allowed the investigation of charged clusters composed of H^+, OH^-, and water molecules. Stillinger and David (1980) used the model to study small ionic clusters of H^+-OH^--H_2O including $H_5O_2^+$, $H_3O_2^-$, and the water octamer. The model uses formal charges of +1 on the proton and -2 on the oxide ion, ensuring the existence of a meaningful reference energy for the reaction $H_2O \rightarrow H^+ + OH^-$. Note that dissociation into ions (also called heterolytic dissociation) is certainly not favored in the gas phase in the absence of aqueous solvent. However, because the model is designed for problems in aqueous chemistry, it was built around the hypothetical heterolytic dissociation energy, which is taken to be 395 kcal/mol. This limits the model to applications involving ionic dissociation (for a parameterized model that reproduces both the homolytic and heterolytic dissociation energies, see Corrales 1999). Besides the dissociation energy, the parameters are chosen so that the equilibrium structure of the water molecule is good by construction.

The ions retain their charges in molecular water, shown in Figure 2. Keeping these charges would result in a model with a very large dipole moment. If these charges are maintained with no other modifications, the dipole moment of a gas-phase water molecule with r_{OH} = 95.84 pm and θ_0 = 104.45° will be 5.64 D. This dipole moment, as

defined by the positions of the ions, is reduced by the polarization of the oxide ion. The interesting feature of the Stillinger-David model is the fact that the H^+ ions polarize the oxide ion, even within the molecule. In general, the polarization of an ion is given by $\vec{\mu} = \alpha \vec{E}$, where $\vec{E}$ is the electric field and α is the polarizability of the ion. For convenience, Stillinger and David took the polarizability of the oxide ion to be 1.444 Å^3, the experimental polarizability of the water molecule, although the exact role of the polarizability in the model is different from that in the experimental measurement. If the oxide ion were subject to the full polarizing power of two protons at a distance of 95.84 pm, the induced dipole would be too large (the total dipole moment, pointing in the opposite direction, would be too small). The idea of the Stillinger-David model is to reduce the OH charge dipole interaction by a function $S(r)$, which approaches 1 at long distances but cuts off the interaction at short distances. Physically, the cutoff function $S(r)$ can be rationalized by covalent bond formation at short range; as the hydrogen ion takes on some electron density within the water molecule, its polarizing power is reduced. The value of the cutoff function $S(r)$ at the equilibrium OH separation in the water molecule is fixed by the dipole moment of water, 1.85 D. This requires that $S(r_e)$=0.4091. The derivatives of $S(r)$ at r_e were estimated by Stillinger and David from experimental information and used to fix other parameters appearing in the functional form for the OH interaction. Note that the reason water is bent in the Stillinger-David model is the reduction in energy of the OH charge dipole interaction obtained by the polarization of the oxide ion.

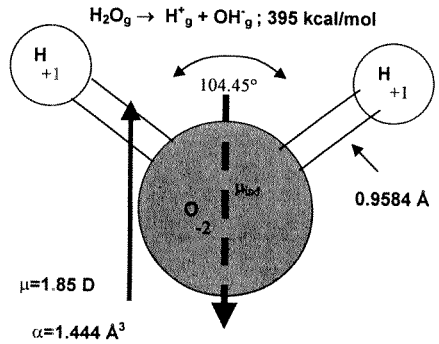

Figure 2. Stillinger-David water model showing formal charges, induced point dipole on oxygen, equilibrium geometry, overall dipole moment, and dissociation energy.

In its original formulation, separate functions were used for the force and the energy, that is, the force was not equal to –grad V. Halley and co-workers (1993) modified the Stillinger-David model to be dynamically consistent. They also added short-ranged bond bending three body interactions to recover exactly the vibrational frequencies of the model. The major modification, however, was in the O-O interaction. In the original Stillinger-David model, the O-O interactions were fixed by what was then known about the water dimer. In the model of Halley et al. (1993), the O-O interactions were fitted to neutron scattering data for the O-O radial distribution function at room temperature (Soper and Phillips 1986).

The functional form of the modified Stillinger-David potential is as follows

$$\Phi_{OO} = \frac{1}{2}\sum_O \sum_{O'} \frac{A_{OO}}{r_{OO'}^{12}} + \frac{B_{OO}}{r_{OO'}^{6}} + \frac{q_O q_O}{r_{OO'}} + \frac{q_O(\vec{\mu}\cdot\vec{r}_{OO'})}{r_{OO'}^{3}} + \frac{1}{2}\vec{\mu}_O\left(\bar{I} - \frac{3\vec{r}_{OO'}\vec{r}_{OO'}}{r_{OO'}^{2}}\right)\vec{\mu}_{O'} \qquad (1)$$

where $\vec{r}_{ij} = \vec{r}_i - \vec{r}_j$, $\bar{I}$ is the 3×3 unit matrix, and $\vec{\mu}_O$ is the dipole vector on the oxygen. The functional form of the O-H interaction is

$$\Phi_{OH} = \sum_O \sum_H a_{OH} \frac{e^{(-b_{OH} r_{OH})}}{r_{OH}} + \left\{ c_{OH} (r_{OH} - r_{0_{OH}})^2 - d_{OH} (r_{OH} - r_{0_{OH}}) \right\} e^{-e_{OH} (r - r_{0_{OH}})^2} + \frac{q_H q_O}{r_{OH}} + \frac{q_H (\vec{\mu}_O \cdot \vec{r}_{OH})}{r_{OH}^3} S_{OH}(r_{OH}) \quad (2)$$

where

$$S(r) = \frac{r^3}{r^3 + f(r)} \quad (3)$$

and

$$f(r) = \frac{f_{OH}(r - r_O) e^{-g_{OH}(r - r_0)} + h_{OH} e^{-p_{OH} r}}{1 + e^{s_{OH}(r - t_{OH})}} \quad (4)$$

H-H interactions are purely coulombic:

$$\Phi_{HH} = \frac{1}{2} \sum_H \sum_{H'} \frac{q_H q_H}{r_{HH'}} \quad (5)$$

For water molecules, there is a three-body term of the form

$$\Phi_{HOH} = \sum_O \sum_H \sum_{H'} \left\{ \begin{array}{l} a_{HOH} (r_{OH} - r_{0_{OH}})(r_{OH'} - r_{0_{OH}}) + \frac{1}{2} b_{HOH} (\theta - \theta_0)^2 \\ + c_{HOH} (r_{OH} + r_{OH'} - 2 r_{0_{OH}})(\theta - \theta_0) + d_{HOH} (\theta - \theta_0) \end{array} \right\} e^{e_{HOH} \left[(r_{OH} - r_{0_{OH}})^2 + (r_{OH'} - r_{0_{OH}})^2 \right]} \quad (6)$$

where $r_{0_{OH}}$ and θ_0 are the desired bond length and bond angle in the water molecule. These parameters are chosen such that the isolated water molecule has the correct vibrational frequencies. Table 1 lists the potential parameters in units of e (charge), Å (length), and e^2/Å (energy). The dipole moment, dissociation energy, and equilibrium structure are used to construct the model.

The model then was used to predict the gas-phase proton affinity of water, which played no part in the model parameterization. This is a fairly rigorous test, as one is faced with computing the energy of a covalent bond based on an ionic parameterization of the structure and dissociation energy of water into ionic fragments. The proton affinity of water, involving an association between a charged species and a neutral species, is much harder to reproduce, for an ionic model, than the energy of dissociation into ions. The modified Stillinger-David model predicts 163 kcal/mol, which is about 8.6 kcal/mol lower than the ΔE_{elec} at the coupled cluster level and at the complete basis set limit (Peterson et al. 1998). This is remarkably good considering the simplicity of the model. The H-O-H angles in H_3O^+ are predicted to be nearly 100°, whereas the angles calculated using the best MO methods are 110°. The hydroxide affinity of water, the energy for the reaction $H_3O_2^- \rightarrow H_2O + OH^-$, is 38.1 kcal/mol. This compares with 37.6 at the DFT BP/DZVP2 level. It is interesting that an essentially ionic model gives such reasonable results for minimum energy structures and energetics.

IRON-WATER AND SILICON-WATER POTENTIALS AND THE BEHAVIOR OF Fe^{3+} AND Si^{4+} IN THE GAS PHASE AND IN AQUEOUS SOLUTION

As a first step in extending the Stillinger-David approach to mineral systems, an Fe-O and Si-O potential was introduced (Rustad et al. 1995; Rustad and Hay 1995). The basis for parameterization of the Fe-O potential was the Fe^{3+}-H_2O potential surface calculated in Curtiss et al. (1987). The surface is given in Figure 3.

Table 1. Parameters for the molecular statics model of the magnetite surface.

A_{OO}	2.02	a_{HOH}	-0.640442
B_{OO}	1.35	b_{HOH}	0.019524
		c_{HOH}	-0.347908
a_{OH}	10.173975	d_{HOH}	-0.021625
b_{OH}	3.69939	e_{HOH}	16.0
c_{OH}	-0.473492	θ_{0HOH}	104.45°
d_{OH}	0.088003		
e_{OH}	16.0	A_{FeO}	1827.1435
f_{OH}	1.3856	B_{FeO}	4.925
g_{OH}	0.01	C_{FeO}	-2.136
h_{OH}	48.1699	D_{FeO}	-74.680
p_{OH}	3.79228	E_{FeO}	1.0
s_{OH}	3.0	F_{FeO}	1.8
t_{OH}	5.0		
r_{0OH}	0.9584	α	1.444 Å^3
		note that the short-ranged FeO parameters are the same for 2.5+ and 3+ sites.	
q_H	1+		
q_O	2-		
q_{Fe}	3+ tet. sites		
q_{Fe}	2.5+ oct. sites		

Note: When used in conjunction with Equations 1–9, energies in e^2/Å are generated. For reference, the water molecule at equilibrium geometry has an energy of 3.11595 e^2/Å; the $Fe(H_2O)^{3+}$ complex has Fe-O = 1.8506 Å, an induced dipole moment μ_O of 0.232222 eÅ (positive side toward the Fe), and a binding energy of 0.48598 e^2/Å relative to Fe^{3+} and H_2O; the hexaaquo $Fe(H_2O)_6^{3+}$ complex has Fe-O=2.0765 Å, μ_O=.577682 eÅ (positive side toward the Fe), and a binding energy of 2.124873 e^2/Å relative to Fe^{3+} and 6 H_2O.

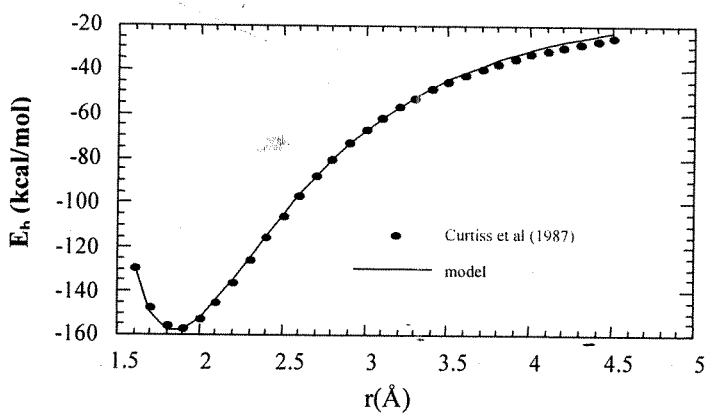

Figure 3. Fe^{3+}-H_2O potential energy surface from Curtiss et al. (1987), and fit from parameterized Fe-O potential function. E_b is the binding energy defined as $E(FeH_2O^{3+})$-$E(H_2O)$ (the energy of Fe^{3+} is zero in the context of the ionic model).

For the Fe-O interactions, the functional form is

$$\Phi_{FeO} = \sum_{Fe}\sum_{O} A_{FeO}e^{-B_{FeO}r_{FeO}} - \frac{C_{FeO}}{r^6} + \frac{D_{FeO}}{r_{FeO}^{12}} + \frac{q_{Fe}q_O}{r_{FeO}} + \frac{q_{Fe}(\vec{\mu}_O \cdot \vec{r}_{FeO})}{r_{FeO}^3} S_{FeO}(r_{FeO}) \quad (7)$$

where

$$S_{FeO}(r) = 1 - \frac{1}{e^{E_{FeO}(r-F_{FeO})}} \quad (8)$$

For the gas phase $Fe(H_2O)_6^{3+}$ ion, the Fe-O bond length is 207 pm, a bit longer than the range of experimental distance of 200-205 pm, with the lower part of the range being the most reliable, having been determined from x-ray diffraction on Fe^{3+} cesium alum (Beattie et al. 1981). Thus one is faced with the question of whether to refit the potential, including not only information from the *ab initio* surface, but also the Fe-O bond distance in the hexaaquo ion. Several issues govern this type of decision. For one, the Fe-O distance is measured in aqueous solution (or, in the case of the Cs alum, in a condensed phase), not in the gas phase. For another, QM calculations on $Fe(H_2O)_6^{3+}$ complexes available at the time also gave Fe-O distances that were too long at 206 pm (Akesson et al. 1994). If the Fe-O distance in the gas phase hexaaquo complex is in error, there is no way of knowing whether the problem is in the Fe-O potential or the water-water potential. Given this second issue, little guidance could therefore be obtained from the quantum mechanical studies in sorting out the right way to improve the model. Furthermore, there is a very strong motivation for keeping the O-O interactions the same for the hexaaquo ion as they are for bulk water. Sacrificing this assumption is unwise as the O-O interaction then becomes dependent on coordination environment, and there will be plenty of instances where there will be no basis at all for assigning coordination-dependent parameters, for example, on surfaces. Taken together, these factors suggest that the simplest approach be used and that one should retain the fit to the *ab initio* surface, leaving the Fe-O bond length in the hexaaquo complex as a prediction of the model based on the Fe^{3+}-H_2O potential surface of Curtiss et al. (1987). The Si-O potential was introduced by fitting to the structure and vibrational frequencies of H_4SiO_4 as calculated by Hess et al. (1988).

The gas-phase acidities of both models were then assessed. The energy required to remove a proton from H_4SiO_4 is 355 kcal/mol, in good agreement with recent DFT calculations (Ferris 1992; Rustad et al. 2000a). The energy required to remove a proton from hexaaquo ferric iron is 40 kcal/mol. This is quite a bit higher than the range of values calculated from *ab initio* theory 20-30 kcal/mol (Rustad et al. 1999a; Martin et al. 1998), but very close to the value calculated for $Al(H_2O)_6^{3+}$ using a variety of *ab initio* methods. The correlation with size-charge ratio for these ions is known to be poor (witness the lesser acidity of the smaller Al^{3+} ion). Despite the fact that DFT calculations were shown to correlate very well with acidities, the electronic structural reasons for the trends observed in the acidities of the trivalent ions are unclear. Until the underlying reasons for these trends are better understood, it seems we should accept the Al^{3+}-like value of 40 kcal/mol, realizing that we are not now really talking about "iron" but a model trivalent ion.

More complex molecules may be used as surrogates for surface sites on oxides. Consider the $Fe_3(OH)_7(H_2O)_6^{2+}$ molecule in Figure 4. This molecule, the simplest polynuclear cluster having an Fe_3OH functional group, was optimized by Rustad et al. (2000b) using density functional theory. The deprotonation energy calculated using the generalized gradient approximation was 179 kcal/mol. Calculations using the molecular

model presented above also gave 179 kcal/mol, showing that the model is capable of giving highly accurate results and is properly accounting for the influence of multiple Fe-O bonds on the acidity of the OH functional group. This provides an immediate point of assessment not available to empirical models such as the MUSIC model, which, because no information is available on the acidities of solution phase functional groups bound to more than one metal, implicitly assumes the additivity of Pauling bond strengths on the surface hydroxide functional groups.

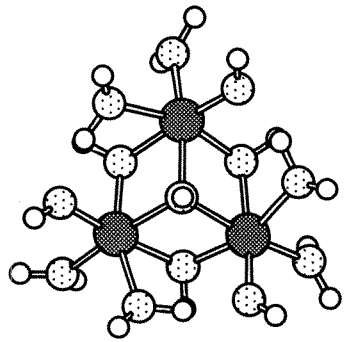

Figure 4. $Fe_3(OH)_7(H_2O)_6^{2+}$ cluster used in the *ab initio* calculation of the gas phase acidity of the Fe_3OH functional group. Large shaded atoms are irons, spotted atoms are oxygen, white atoms are hydrogen.

Both the Si^{4+} and Fe^{3+} potentials yielded qualitatively reasonable behavior when used in a simulation of a single aqueous ion in a solution of 216 water molecules. For the Fe^{3+} system, the potential gave a six-fold coordinated aquo ion $Fe(H_2O)_6^{3+}$. In contrast, the Toukan-Rahman flexible model (Toukan and Rahman 1985) gave an eightfold coordination for the Fe^{3+} in solution when fit to the Fe^{3+}-O interaction fit to the Fe^{3+}-H_2O surface calculated by Curtiss et al. (1987). The improvement in the modified Stillinger-David model is presumably due to the better transferability of the polarizable model. The dipole moment of the Toukan-Rahman water model (2.3 D) is an effective dipole moment that would be changed if the water is not in an environment typical of bulk water. The charge-dipole interaction between the Fe^{3+} ion and the coordinating oxygen nearly nullifies the induced moment, greatly increasing the net dipole moment of the coordinating water molecules. These kinds of many-body effects are important in stabilizing the hexaaquo complex in solution. The Si^{4+} when placed in the 216 water system immediately hydrolyzed four water molecules to make an orthosilicic acid molecule and four hydronium ions. This is reasonable, considering that Si^{4+} is so acidic that its pK_a is not measurable and, at a pH of about 1.7, the orthosilicic acid molecule should not be protonated.

CRYSTAL STRUCTURES

Having established that reasonable results are obtained for the aqueous ions using the simple potential functions, the natural next step is to try the potential functions on crystal structures. This was carried out for goethite, lepidocrocite, akaganeite, and hematite in the Fe^{3+}-O-H system for the structures by Rustad et al. (1996a). Just using the simple parameterization from the single Fe^{3+}-H_2O surface, quite good results were obtained with stable crystal structures for all the FeOOH polymorphs as well as hematite. As with the hexaaquo ion, the Fe-O bonds were about 5% too long. As for the hexaquo complex, it could not be determined whether the long Fe-O bond lengths were primarily a result of the Fe-O interaction being incorrect or the O-O interaction being incorrect.

It might be supposed that the relative energies of the different polymorphs could be used to further test the model. Recent calorimetric studies have provided valuable information on the relative energies of the FeOOH polymorphs. These energies are compared in Figure 5 with calculated potential energies at the optimized lattice and fractional coordinates both for the model derived in Rustad et al. (1995) and also from density

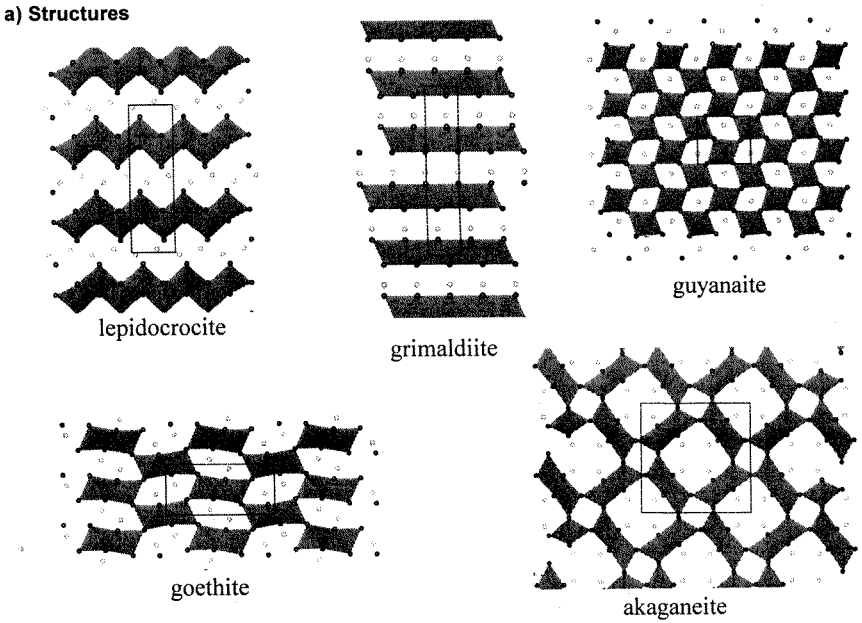

Figure 5 (a) Structures and (b) relative energies of FeOOH polymorphs calculated with parameterized model, plane-wave pseudopotential methods, and experiment (Laberty and Navrotsky, 1998).

functional calculations using CASTEP, taken from Rosso and Rustad (2001). The major conclusion to be drawn is that the relative energies of the FeOOH polymorphs are very close. The ordering of the DFT total energies of the different polymorphs was dependent on whether GGA or LDA was used, with LDA giving the correct ordering of diaspore < boehmite. One concludes that the problem of obtaining theoretically the energy differences among the various polymorphs is beyond current capability of electronic structure methods. It may be that an empirically derived exchange-correlation functional analogous to B3LYP, but parameterized on thermodynamic data on oxides, will be a useful approach in future work.

VACUUM-TERMINATED SURFACES

The next level of complexity is to create a surface from the bulk material. First, it is necessary to choose the type of model to be used to represent a surface. There are two possible choices: (1) a semi-infinite surface (Jones et al. 2000) or (2) a slab. The semi-infinite model uses a two-region approach, whereas the slab model uses 2-D periodic Ewald methods to treat long-range forces. In either case, it is necessary to demonstrate convergence: in the former case, with respect to the partitioning of the two regions; in the latter case, with respect to the thickness of the slab.

Vacuum truncation of an oxide surface produces unusual coordination environments for surface atoms. In the process of producing a molecular model of surface, be it in a vacuum or otherwise, some guess must be made about the surface termination. In principle, this could be arrived at from the simulation itself. One could imagine simulating the crystal growth process of, say, molecular beam epitaxy and allowing the surface structure to evolve from the simulation. One could also start with a bulk crystal and apply a uniaxial tension along the direction of the surface of interest, forcing the crystal to break along the surface of interest but allowing the atomistic structure of the surface to be determined from the simulation. As many vacuum surfaces are produced by sputtering and annealing, one might also attempt to simulate this process. In practice, nearly all surface terminations are arrived at through a combination of common sense and a set of rules defined by Tasker (1979), which basically states that surfaces should be constructed such that they exhibit zero dipole moment. Another way to think of this is that the surface will cleave in such a way as to give the same structure on either side of the cleavage surface. This principle is illustrated in Figure 6 for the (001) surface of hematite.

Much recent experimental work has focused on the structures of vacuum terminated oxide and carbonate surfaces of geochemical interest (Chambers et al. 2000; Thevuthasan et al. 1999; Sturchio et al. 1997; Fenter et al. 2000; Guenard et al. 1998; Charlton et al. 1997). For the (001) surfaces of corundum and hematite, there is good agreement between a variety of theoretical calculations and experimental results, at least in the sense that the gross feature of the surface relaxation, the large inward relaxation of the metal terminated surface, is the same for both the experimental and theoretical models. Parameterized models, quantum mechanical calculations, and experiment all agree that the uppermost Fe layer relaxes inward by approximately 50% after cleavage. However, there are some significant differences between both the *ab initio* and parameterized models and experiment. For example, in Table 2, we see that the theoretical methods agree well with each other, but may underestimate or overestimate the relaxation in the layers underneath the top layer.

Magnetite (001) is geochemically relevant and, because magnetite is a good conductor, is also amenable to various high vacuum techniques requiring good sample

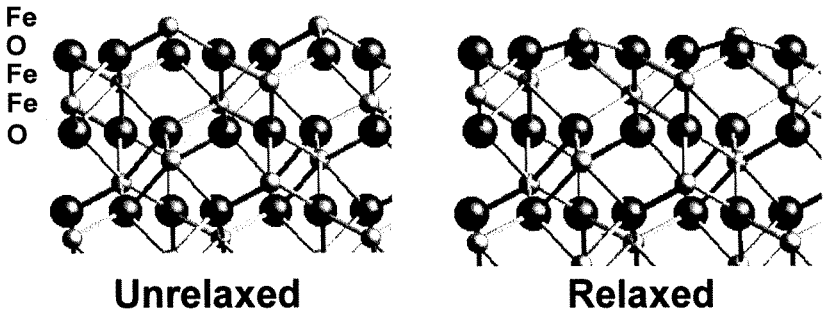

Figure 6. Relaxation of corundum (001). Small atoms are metals, large atoms are oxygens. (a) Bulk structure showing cleavage plane between adjacent iron layers, (b) Relaxation of top iron layer into the surface.

Table 2. Percent change in z component upon relaxation after cleavage of hematite along (001) as shown in Figure 6.

	XPD [a]	*GIXS* [b] *(Al_2O_3)*	*Model* [c]	*LAPW* [d]
Fe	-41	-51	-49	-57
O	+18	+15	-3	+7
Fe	-8	-29	-41	-33
Fe	+47	+18	+21	+15
O				

[a] X-ray photoelectron diffraction on hematite (001) from Thevuthasan et al. (1999)
[b] Grazing incidence x-ray scattering on Al_2O_3 (001) from Guenard et al. (1998)
[c] Calculations on hematite (001) from Wasserman et al. (1997)
[d] Linearized augmented plane wave calculations from Wang et al. (1998)

conductivity. The spinel structure may be represented as a sequence of neutral stacking units parallel to (001) as shown in Figure 7. This stacking sequence builds up the octahedral (B layer) and tetrahedral (A layer) sites characteristic of the spinel structure. The unit cell of the stacking layer is $(\sqrt{2}\times\sqrt{2})R45$ relative to the bulk. In the bulk, a tetrahedral atom, coming from the overlying stacking unit, is bonded to the oxygens at the center of the unit cell. This shrinks the cell by a factor of $1/\sqrt{2}$ and rotates the cell by 45°. In magnetite, Fe^{3+} occupies the tetrahedral sites, while the octahedral sites are filled with an equal mixture of Fe^{2+} and Fe^{3+}. Above the Verwey temperature (119 K), the electrons in the rows of octahedral B sites are delocalized; these sites may be thought of as being occupied by $Fe^{2.5+}$ ions. Termination of the stacking sequence in Figure 7 will result in a neutral, stoichiometric, autocompensated surface with two-fold coordinated Fe^{3+} and five-fold coordinated $Fe^{2.5+}$ sites (Kim et al. 1997). This surface is referred to as the tetrahedral or "A" layer termination. It was found in Rustad et al. (1999c) that the two-fold coordinated Fe^{3+} ions at the surface are unstable in their bulk positions and rotate downwards to occupy the adjacent five-fold half octahedral site in the plane of the B layer. This relaxation mechanism is illustrated in Figure 8. This was rationalized in

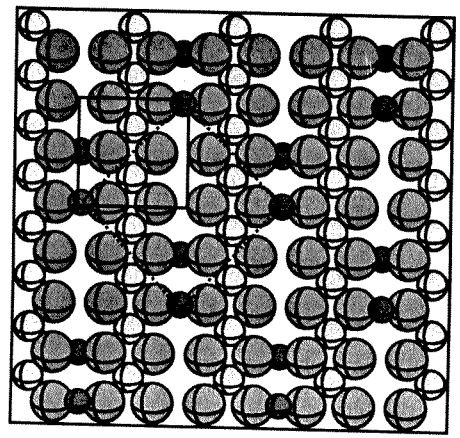

Figure 7. Neutral stacking sequence generating magnetite parallel to (001) large medium gray atoms are oxygens, small light gray atoms are octahedral irons, small dark atoms are tetrahedral irons. Bulk unit cell is shown by the solid box; the surface unit cell is shown by the dashed box.

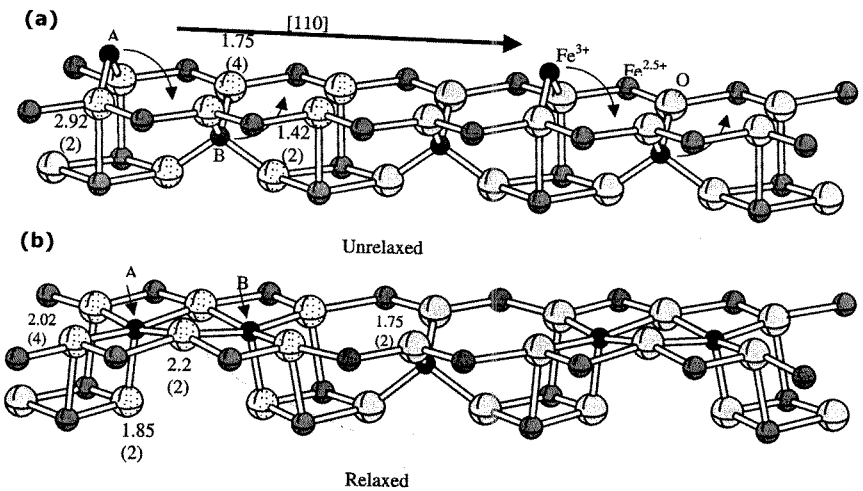

Figure 8. Relaxation of vacuum terminated magnetite (001) according to Rustad et al. (1999). (a) unrelaxed structure assuming $(\sqrt{2}\times\sqrt{2})R45$ termination in Kim et al. 1997), down [110] direction as indicated in the Figure. (b) relaxed structure. Only a single row between the 2.5+ sites is shown. Tetrahedral sites are dark, small ions, octahedral 2.5+ sites are medium gray ions, and large light ions are oxygens.

terms of the driving force resulting from the overcoordination of the oxygens attached to the two-fold coordinated Fe^{3+} in terms of Pauling's rules. This surface structure provides a compelling interpretation of STM images of magnetite (001), where curious dimeric structures were observed in between the $Fe^{2.5+}$ rows along [110]. The observation of "dimers" would then simply result from the second layer tetrahedral Fe^{3+} being pushed up to the surface in response to the relaxing first layer tetrahedral Fe^{3+}. Recent experiments, however, have been more consistent with a bulk termination without extensive surface relaxation. It is possible that the discrepancy results from full oxidation

of the surface ions, in which case the MD model does not relax as in Figure 8. This interpretation does not provide a ready explanation of the STM images; however, it may be possible that probing the surface structure with the STM changes the oxidation states of the surface sites, allowing the relaxation mechanism in Figure 8.

Two important aspects of vacuum-terminated surfaces are 1) the extent of surface relaxation upon cleavage of the crystal structure across the surface and 2) the energy required to cleave the crystal. Under vacuum conditions, only the surface relaxation is accessible to experiment. Measurements of cleavage energies, at least for the oxide crystals of interest in the work described here, are exceedingly difficult and have not produced convincing results. These energies are readily calculated theoretically, however, and this provides an important connection between quantum mechanical and parameterized methods. The surface energy is defined by

$$\sigma = \frac{(E_{slab} - E_{bulk})}{2A} \tag{9}$$

where E_{slab} is the total energy of the slab and E_{bulk} is the energy of an equivalent number of atoms in the bulk crystal. This equation assumes that the slab is stoichiometric. Nonstoichiometric slabs are possible if changes take place in redox state. The basic approach used for nonstoichiometric slabs is described in Wang et al. (1998). To illustrate the general idea, let us define the slab free energy of an iron oxide surface at zero temperature and pressure (so both PV and TS are zero) as

$$\Omega_{slab} = E_{slab} - N_{Fe}\mu_{Fe} - N_O\mu_O \tag{10}$$

Consider specifically a magnetite slab. In addition to the "A" termination discussed above, another termination has been postulated (Voogt 1998) and observed with scanning tunneling microscopy investigations (Stanka et al. 2000). As this termination involves the removal of FeO from the "A" terminated surface, the relative stabilities of the two surfaces will depend on the partial pressure of oxygen in the system. Rustad et al. (2000c) analyzed the relative stabilities of these surfaces using the molecular model presented above. Because of the interdependence between the chemical potentials of magnetite, oxygen, and iron

$$\mu_{Fe} = \frac{1}{3}\mu_{Fe_3O_4} - \frac{4}{3}\mu_O \tag{11}$$

Equation (10) may therefore be rewritten:

$$\Omega_{slab} = E_{slab} - \frac{1}{3}N_{Fe}\mu_{Fe_3O_4} + (\frac{4}{3}N_{Fe} - N_O)\mu_O \tag{12}$$

At zero pressure and zero temperature, the first two terms are just E_{slab}-E_{bulk}, similar to Equation (9) except that we have not yet divided out the surface area. The last term is zero if the slab is stoichiometric magnetite. If the stoichiometry is different from magnetite, however, the free energy of the slab will depend on the partial pressure of oxygen in the system. If the surface is oxidized relative to magnetite ($N_O > {}^4/_3 N_{Fe}$), the surfaces chemical potential will decrease with pO_2, if it is reduced, the chemical potential will increase with pO_2. Wang and coworkers (1998) were able to calculate the chemical potential of O_2 gas directly using DFT methods. Rustad et al. (2000c) used an indirect approach in which the differences in total energies of bulk FeO, Fe_3O_4, and Fe_2O_3 were used to fix the μ_O values at the magnetite-hematite, magnetite-wustite, and wustite-hematite buffers. This allowed the establishment of an empirical relation between μ_O and pO_2 that could be used to evaluate Equation (11) allowing the relative stabilities of slabs

having different oxidation states to be calculated as a function of the oxygen pressure. Calculations on charge-ordered magnetite slabs indicate that, within the context of the ionic model presented here, the surface energy of the "A" termination of magnetite is lower than that of the "B" termination over a wide range of oxygen fugacities (Rustad et al. 2000c). Hydroxylation has a negligible effect on the relative energies of the "A" and "B" surfaces.

HYDRATED AND HYDROXYLATED SURFACES

Neutral surfaces

The next level of complexity involves hydrating the vacuum terminated surface with a single layer of water. Hydration and hydroxylation of mineral surfaces have received significant attention in both theoretical and experimental investigations. Many studies have focussed on the energy difference between molecular and dissociative adsorption of water (Lindan et al. 1996; Stirniman et al. 1996; Wasserman et al. 1997; Langel and Parrinello 1994; Giordano et al. 1998; Henderson et al. 1998; Shapalov and Truong 1999). This energy difference is a direct reflection of the acidities and basicities of surface functional groups. Dissociative water adsorption will be favored for acidic $=MO_{ad}H_2$ functional groups and basic M_nO_{lat} where O_{ad} represents the oxygen of an adsorbed water molecule and O_{lat} represents a lattice oxygen. Other things being equal, the acidities of $=MOH_2$ functional groups would be expected to be proportional to the size to charge ratio of the metal and the coordination number (Parks and deBruyn 1962; Parks 1965; Yoon 1979; Hiemstra et al. 1989). The process of surface hydration was indicated in Figure 1.

Hydroxylation energies, defined as the difference between the vacuum-terminated surface energy (Eqn. 8) and the adsorption energy of water, are negative for minerals in the iron oxide system discussed here. This means that the crystal would prefer to break apart and hydroxylate rather than remain whole in the presence of aqueous solution. This is wrong, as experimental studies have shown that the *enthalpy* of dissolution of goethite decreases (becomes more negative) as total surface area increases. There may be important entropic and zero-point effects, but, taken at face value, this indicates that either the dry cleavage energy is too easy or that the binding of the water to the undercoordinated iron ions on the surface is too large. Although *ab initio* calculations agree well with the cleavage energies obtained by the classical model discussed here for hematite (001), we have shown that plane-wave pseudopotential calculations also give negative hydroxylation energies for Al_2O_3 (see Fig. 9).

Several experimental techniques can be used to examine the extent of water dissociation on a mineral surface. One of the most informative is the simple temperature programmed desorption experiment (Masel 1996). In this experiment, a sample is placed in a vacuum chamber at low temperature, and a measured amount of water vapor is introduced. The sample is then heated at a definite rate and the amount of water vapor desorbing from the sample is measured as a function of temperature. In general, the desorption is not uniform with temperature, and several TPD "states" are manifested as maxima in the flux off the sample. These experiments are performed under several water doses. At very high doses, a maximum at 160 K is observed independent of the substrate. The presence of this 160 K "ice peak" indicates the formation of multiple layers of ice forming on the sample. As the exposure is decreased to one monolayer, this peak gradually disappears. Peak positions may change with coverage.

This experiment in principle provides a "fingerprint" of the energies of various sites for water binding on an oxide surface. In practice, interpretation of TPD data can be

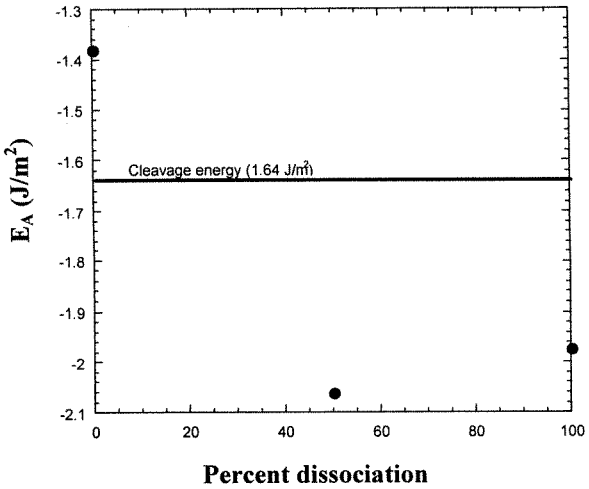

Figure 9. Adsorption energies for water on the α-Al_2O_3 as a function of the extent of dissociation on the surface. The cleavage energy is represented by the solid line at 1.64 J/m^2, implying that the crystals are unstable. Zero point energies are not considered.

difficult; in a typical experiment, both the coverage and the temperature are changing at the same time. For example, consider Figure 10 taken from Henderson et al. (1998) on the hematite (012). One observes one peak at 260 and another at 350 K. One possible interpretation of this data is that the low-temperature peak represents a small amount of molecularly adsorbed water, and the high-temperature peak represents the recombination of OH and H of water molecules that have dissociatively adsorbed to the surface. The problem with this interpretation is that the 350 K peak is independent of coverage. This is not typical of recombinative desorption; at lower coverages, the recombining species have less frequent encounters, and the desorption temperature should increase.

This observation, along with other evidence from secondary ion mass spectrometry experiments, lead to more detailed consideration of the calculated hydration/hydroxylation energies for hematite (012) reported above. In particular, it would be interesting to know hydration energies at intermediate points between 0, 50% and 100% dissociation. Perhaps there were low configurations having 10% or 20% dissociation that were lower in energy than the 50% dissociated configuration. Rustad et al. (1999b) considered a 2×2 supercell, containing eight adsorbed water molecules. The results of these calculations are shown in Figure 11, essentially confirming the extensive dissociation predicted by the model for the 1×1 cell. The larger scale investigations predicted 75% dissociation. Even with these modest cell sizes the number of proton configurations becomes enormous. In the particular case of hematite (012), we examined 1,296 possible proton configurations. This number could have been reduced by nearly a factor of two by accounting for symmetry, but this still leaves approximately 650 possible proton configurations, each of which would ideally require a conformer searching procedure to find the lowest energy tautomers. This is well beyond what would be possible with *ab initio* methods unless they were "grand-challenge" types of efforts. The hydroxylation problem is essentially a rare-events problem in that the barriers to proton motion are large. Even in a full MD simulation with solvent present, one cannot reasonably expect to let the system naturally sample all protonation states by itself. Conformer searching by molecular dynamics techniques on this scale is not a reasonable proposition with Car-Parrinello methods at the present time.

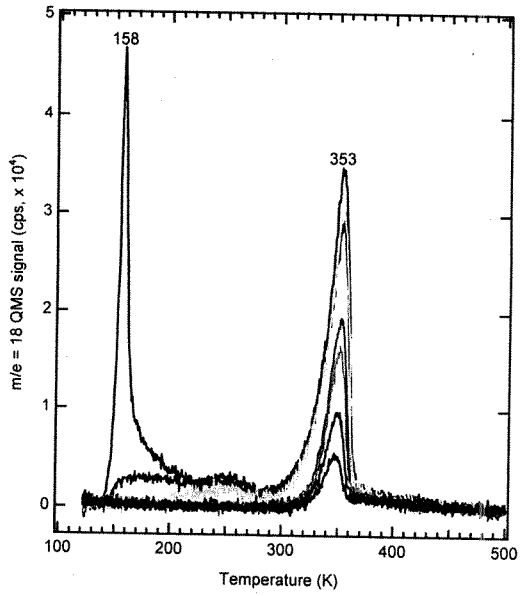

Figure 10. Temperature programmed desorption curve of water on hematite (012) from Henderson et al. (1998) at various coverages. Peak at 158 K is from ice formed at coverages in excess of 1 monolayer. Note first-order coverage-independent behavior of desorption peak at 353 K.

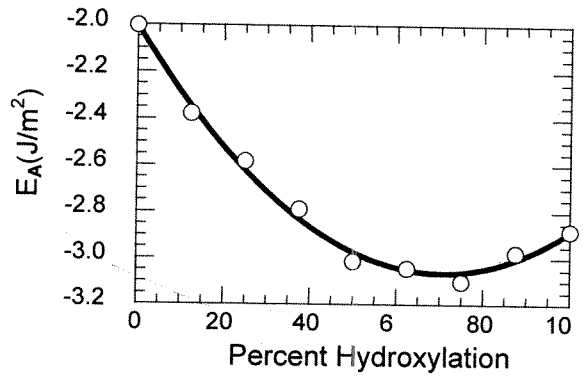

Figure 11. Adsorption energy as a function of percent hydroxylation calculated from energy minimization studies using the model on hematite (012). Cleavage energy is close to 2 J/m^2. Each point on the curve represents the lowest energy structure at each point on the x axis, taken from 1,296 total energy minimizations.

Additional experiments using isotopically-resolved TPD and vibrational spectroscopy using HREELS have confirmed the theoretical calculations of approximately 75% water dissociation on hematite (012). In the isotopically resolved TPD experiments, O^{18} water was deposited on a bulk terminated hematite (012) surface made with O^{16} (by annealing in O^{16} gas). The peak at 350 K at monolayer coverages comprises approximately equal mixtures of O^{18}-O^{16}, almost surely requiring that the water dissociate. HREELS work showed the presence of δ Fe-OH vibrations at 960 cm^{-1}, indicative of dissociated water. Regarding the first-order behavior of the TPD spectrum,

one straightforward explanation is that the hydroxyls are not mobile on the surface. The water arrives at the surface and dissociates, and both hydroxyls are essentially immobile until they recombine upon desorption.

The mixing of the lattice and adsorbed oxygens serves as proof of water dissociation but is troubling nonetheless. One problem is that given the canonical surface structure one is faced with exchanging the Fe_3OH and FeOH sites, as shown in Figure 12, which would be expected to have a very high barrier of activation energy. Another problem is that this is supposed to happen without the dissociated products being mobile enough to yield second order behavior of the 350 K TPD peak. Remember that this exchange is pervasive and is not happening only at defects. One possible hypothesis is that some mobile defect is present which, like a plow, mixes up the adsorbed and lattice oxygens as it migrates through the surface. Another possible interpretation is that the vacuum structure of the surface is wrong altogether, and, in fact, the true structure contains a singly-coordinated Fe-O group. This would give rise to a mixed desorption peak because after adsorption of water, equivalent Fe-$O_{lattice}$H and Fe-$O_{adsorbed}$H groups exist on the surface. LEED patterns show that the surface structure is 1×1, but this does not mean that the surface has the simple bulk-terminated structure.

To help resolve this issue, Bylaska and Rustad (unpublished) have carried out *ab initio* Car-Parrinello simulations of the canonical surface in the Al_2O_3 system. They did not observe any structural rearrangements to configurations with Al-O groups, nor did they observe any reconstructions on the hydrated surface that could explain the mixing. These authors chose to work with the analog Al_2O_3 in these calculations because of the complications of treating transition metals with plane-wave pseudopotential methods. The analogy may not be valid; the mixing experiments on the Al_2O_3 (021) surface have yet to be performed. Suffice it to say that although we have agreement between theory and experiment about the extent of dissociation of water on hematite (021), some fundamental pieces of the puzzle are still missing. Similar difficulty exists for the (001) surface of Al_2O_3 (Nelson et al. 1998; Hass et al. 2000), but this is less surprising given the relative complexity of the (001) relaxation.

For the magnetite (001) surface, calculations were carried out on three sets of hydroxylated slabs, including both the relaxed and unrelaxed "A" terminations and the "B" termination (Rustad et al. 2000c). For the "A" termination, four waters are added per

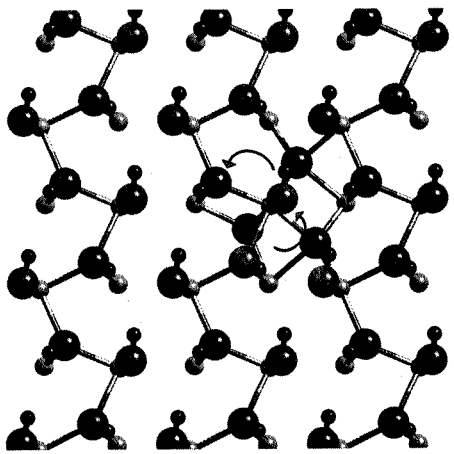

Figure 12. Hydroxylated (012) surface of α–Al_2O_3 from ab initio molecular dynamics simulation (Bylaska and Rustad, unpublished). Arrows show the mixing that must somehow take place during isotopic mixing.

unit cell to the octahedral sites and two waters per unit cell are added to the tetrahedral sites (see Fig. 13). Assuming each of the sites has at least one proton, there are 12!/(6!×6!) = 924 possible tautomers for each unit cell. An exhaustive search through these possible tautomers yielded the structure shown in Figure 13 as the lowest-energy tautomer. Because of the large number of tautomers within the unit cell, it was not possible to examine arrangements outside the k = 0 (all unit cells the same) approximation as was done for hematite (012) (Rustad et al. 1999b). Total water binding energies for both surfaces were about 2.32 J/m^2, indicating that the presence of water will have little effect, at least in a thermodynamic sense, on which surface is observed.

It is of interest that the unrelaxed "A" terminated surface is lower in energy than the relaxed "A" surface upon hydroxylation; the presence of water in the system should "undo" the surface relaxation predicted in Figure 8. This in fact explains an apparent paradox suggested by temperature-programmed desorption studies on magnetite (001) (Peden et al. 1999). These investigators showed the existence of three peaks in the (001) TPD spectrum at 225 K, 260 K, and 325 K. Each peak contributes approximately equal amounts to the TPD spectrum. In one possible interpretation, the 225 K and 260 K peaks are contributed by octahedral Fe^{2+} and Fe^{3+} sites, while the peak at 325 K is coming from the Fe^{3+} tetrahedral sites. The octahedral 2.5+ site would be charge-ordered in this interpretation. An objection to this interpretation is that one would not expect the two waters on the tetrahedral sites to desorb at the same temperature. Once one of the waters has desorbed, the remaining water should be held more tightly, as the surface Fe^{3+} is now only threefold coordinated. It seems reasonable to expect two peaks at high temperature because the desorbing waters are coming from the same site.

This puzzling lack of two peaks at high temperatures can be rationalized by calling on the large surface relaxation energy to reduce the binding energy of the final water removed from the surface. Calculation of binding energies for each of the waters on the tetrahedral sites shows that the binding energy of the second water (43 kcal/mol) is in fact the same as that of the first (44 kcal/mol). The similarity in binding energies arises because the "A" surface relaxation mechanism is not accessible until the second water is removed from the surface. After this water is desorbed, the system gains 0.72 J/m^2 of

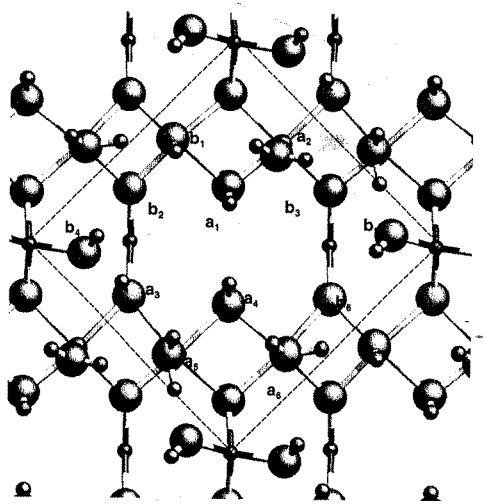

Figure 13. Surface sites on hydroxylated magnetite (001). "a" sites are acid/donor sites. "b" sites are basic/acceptor sites. Large atoms are oxygen, small dark atoms are iron, small light atoms are protons.

surface energy in relaxation, thus decreasing the total binding energy of the second water to a value very close to that of the first water.

Surface charging

One of the oldest and most fundamental experiments on solvated oxide surfaces is the measurement of the amount of charge accumulated on the surface as a function of the pH of the solution. This is closely related to the issue of the dissociation of water on the hydrated surface discussed in the previous section. There is a close relationship between surface and aqueous hydrolysis. Aqueous hydrolysis reactions are structurally much less ambiguous than surface hydrolysis reactions and therefore are useful in the interpretation of surface hydrolysis data. This concept is fundamental and goes back to the pioneering work of Parks and deBruyn (1962).

As pointed out by Hiemstra et al. (1989), the main difficulty of this approach is that all aqueous hydrolysis data are based on mononuclear MO, MOH, MOH_2 functional groups whereas surfaces also will have bi- and tri-nuclear surface functional groups such as M_2OH and M_3OH. Other obvious differences are that solvation effects would presumably be very different between surfaces and aqueous complexes, and internal solid-state relaxation effects are absent entirely.

The obvious approach to using molecular modeling to address surface charge is to calculate the energies required to remove protons from the neutral surface and the energies gained by adding protons to the neutral surface. In periodic slab systems, the repeating cell must be neutral overall to define the potential energy using the Ewald summation. Therefore, the calculation actually performed is, in the case of loss of a proton, the energy of moving the proton from a localized positive charge to a positive charge dispersed uniformly throughout the 2-D periodic plane defining the unit cell of the slab (see Fig. 13). This quantity is sufficient to calculate relative values of proton affinities or gas-phase acidities within the same cell as the energy of the uniform compensating charge can be shown to be independent of the positions of the atoms in the cell. There is, however, a systematic dependence of the deprotonation/protonation energies arising from defect-defect interactions across image cells which should be taken into account (Wasserman et al. 1999 and references therein).

To illustrate the gas-phase proton binding approach to calculating logK for the surface charging, the neutral surface of magnetite (001) is shown in Figure 14. To simplify the task of assigning locations for proton addition and removal, assume protons are added in such a way as to maintain the Pauling bond strength at the oxide ion in the range $-1<0<1$. Pauling bond strength (PBS) is defined as $\Sigma Z_i/CN_i$ where Z is the charge of the ith coordinating cation and CN is the coordination number of the ith coordination cation. Therefore, we eliminate surface species such as Fe_3OH_2 (PBS=+3/2) or FeO (PBS=-3/2). The various surface sites and their associated energy changes (positive for proton removal, negative for proton addition) are shown in Table 3. Also shown in Table 3 are the predictions from the revised MUSIC model (Hiemstra et al. 1996). Because of the sensitive dependence of the site acidity on bond length, the MUSIC model predicts that the triply coordinated $=Fe^{oct}{}_2Fe^{tet}OH$ sites and the singly-coordinated $Fe^{tet}OH_2$ are much more acidic than would be indicated by the relative gas-phase acidities. The molecular model does recover the differences on bond length between the $Fe^{tet}OH$ and $Fe^{oct}OH$ bonds, but the influences on the gas-phase acidities are not systematic.

To make some prediction about an experimentally measurable quantity, like the pH of zero charge, requires that some relationship be developed between the gas-phase proton affinities and acidities of surface sites and their associated pK_as in solution. To do this, we used the classic method of correlating the known pK_as of aqueous species with

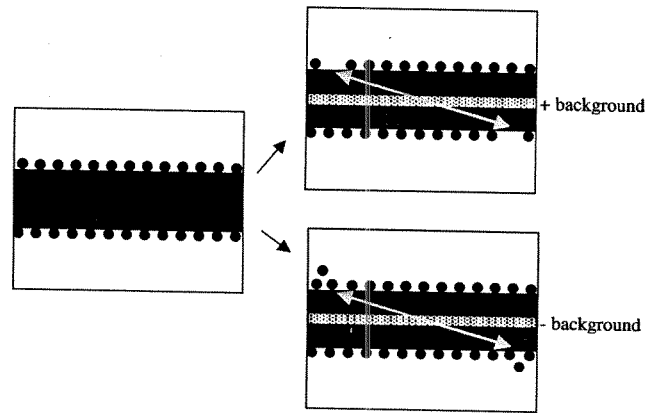

Figure 14. Protonation/deprotonation of neutral slab in periodic boundary conditions. Slab remains neutral due to addition of uniform positive (deprotonation) or negative (protonation) background charge. The energetic contribution from the uniform charge does not depend on the positions of the atoms, only on the size and shape of the unit cell.

Table 3. Sites present in Figure 13.

Site	*Site Type*	*Fe-O bond lengths (Å) on neutral surface* Bulk: $Fe^{3+}O$=1.94 $Fe^{2.5+}O$=2.12	*GPA GPPA*	*LFER pK_a*	*CD-MUSIC*
Acceptor Sites					
b_1	$Fe^{2.5+}OH$	2.09	-340	10.2	11.5
b_2	$Fe^{2.5+}{}_2Fe^{3+}O$	1.99, 2.06, 1.84	-352	10.5	4. 5
b_3	$Fe^{2.5+}{}_2Fe^{3+}O$	2.02, 1.97, 1.89	-343	10.3	4. 5
b_4	$Fe^{3+}OH$	1.90	-343	10.3	5.1
b_5	$Fe^{3+}OH$	1.91	-340	10.2	5.1
b_6	$Fe^{2.5+}{}_2Fe^{3+}O$	2.06, 2.01, 1.85	-352	10.5	4. 5
Donor Sites					
a_1	$Fe^{2.5+}{}_3OH$	2.13, 2.08, 2.14	307	9.3	10.9
a_2	$Fe^{2.5+}OH_2$	2.17	288	8.7	11.5
a_3	$Fe^{2.5+}{}_2Fe^{3+}OH$	2.02, 2.21, 2.14	288	8.7	4. 5
a_4	$Fe^{2.5+}{}_3OH$	2.19, 2.11, 2.10	311	9.4	10.9
a_5	$Fe^{2.5+}OH_2$	2.21	288	8.7	11.5
a_6	$Fe^{2.5+}OH_2$	2.16	288	8.7	11.5

Note: Sites are listed by donors and acceptors. The list includes site type as identified by coordinating metal ions and protons, the bond lengths to the coordinating Fe ions, the gas-phase acidity/gas-phase proton affinity (GP/GPPA), the log K for the reaction using the relationship from Rustad et al. (1996), and the prediction of the revised MUSIC model described in Hiemstra et al. (1996). MUSIC model predictions are given in terms of proton loss from protonated acceptor sites, for example FeOH in the acceptor list and $FeOH_2$ in the donor list imply the same reaction and have the same pK_a. Bond lengths are those predicted by the molecular dynamics model discussed here, which are systematically too long by about 5%.

some calculated quantity and applying the same relationship to surface species. In Rustad et al. (1996b), gas-phase acidities for $Fe(H_2O)_6^{3+}$ -$Fe(OH)_3(H_2O)_3$ were calculated using the model. The calculated acidities were correlated with the solution pK_as, and this correlation was used to predict solution pK_a for the surface species. This correlation was subsequently empirically modified by Felmy and Rustad (1998) to get a somewhat better fit to the surface charging data at multiple ionic strengths.

Applying the correlation from Felmy and Rustad (1998) to magnetite gives the surface pK_as listed in Table 3. The prediction using the LFER derived from molecular modeling incorrectly predicts a basic surface. The PZC of the (100) surface predicted by the MUSIC model, however, is in good agreement with experiment (see also estimates by Wesolowski et al. (2000)). I make the bold claim that the MUSIC model is getting the right answer for the wrong reason, and that the model of Rustad et al. (1996b) gets the wrong answer for the right reason. This may be difficult to accept, especially given the ease of use of the MUSIC model (requiring only paper and pencil) and its great generality of application (nearly the entire periodic table).

In defense of the molecular model, it must be pointed out that it has successfully explained experiments on the simpler systems described above. Of particular relevance here is the amount of water dissociation on hematite (021), the relaxation of hematite (001), and the agreement with quantum mechanical calculations of the gas-phase acidity of the trimeric $Fe_3(OH)_7(H_2O)_6^{2+}$ polynuclear cluster. These calculations taken together suggest that the model can correctly deal with both structural and energetic characteristics of the triply coordinated surface oxygens. It is true that the model has been somewhat controversial on magnetite (001), but even if it fails here, it is because of the complex electronic structure of magnetite. This should also cause anomalies in the MUSIC model. The empirical MUSIC model was not designed to make any predictions about these simpler systems and cannot be tested in these less complicated proving grounds.

It is worth emphasizing that the arguments leading up to the construction of the MUSIC model are gas-phase arguments based on "ionic" concepts such as Pauling bond order. This essential physics is present in both approaches. It cannot be argued that the MUSIC model is accounting for subtle quantum mechanical effects not present in ionic model because the MUSIC model rests entirely on an ionic framework.

To advocate this line of reasoning, there must be a convincing explanation of the cause of the disagreement with experiment. There are two possibilities: 1) aqueous solvent effects, and 2) electronic structural effects not accounted for by the ionic model of magnetite. Relevant to this second point is the recent work of Sverjensky (1994) and Sverjensky and Sahai (1996). These authors emphasized the role of the mineral dielectric constant in determining mineral surface reactivity. According to their model, the major reason for the enhanced acidity of magnetite is its high dielectric constant, which was shown to be positively correlated with site acidity, other things (like Pauling bond orders) being equal. A possible physical explanation is that if the distribution of cation charges rearranges itself in response to surface deprotonation, the relaxation energy is large, and this makes the mineral is more acidic. The same thing is true of excess positive charge added to the surface, but, since the adsorbed positive surface charge should be "further away" from the bulk, it elicits less of a response than positive charge removed from the neutral surface, which should be closer to the bulk mineral.

The problem with this argument, in the case of magnetite, is that maghemite (γ-Fe_2O_3), which has effectively the same structure as magnetite, but without mobile electrons giving rise to a large dielectric constant, should be less acidic than magnetite. There have not been many studies, but it appears that maghemite has about the same

acidity as magnetite (Watanabe and Seto 1990). Also, if bulk relaxation effects caused the high acidity of magnetite, it might be expected that this would be evident in the TPD experiments on magnetite, perhaps giving rather high binding temperatures due to the increased "solvation" of the protons and OH groups on the surface. Recent TPD experiments on magnetite (001) by Peden et al. (1999) as discussed above give OH recombination TPD peaks at roughly the same temperatures as seen by Henderson et al. (1998) on hematite (012), showing no evidence of enhanced retention of either the molecular or dissociated products. Furthermore, spin-polarized STM studies (Wiesendanger et al. 1994) indicate that the effective Verwey temperature of the surface of magnetite may be much larger than that of the bulk. This results from surface induced band-narrowing, giving rise to a lesser degree of quantum "delocalization" energy, which tends to trap the electrons on Fe^{2+} sites. It is emphasized that these arguments apply to one case only (magnetite), and that the above arguments are not intended to call into question the general utility of considering the mineral dielectric constant in surface complexation theory. In the particular case of magnetite, then, the remaining issue is the effect of aqueous solvent. This brings us to the final section on solvated systems although the issue is by no means resolved here.

SOLVATED INTERFACES

Calculations on solvated systems are very expensive computationally, even for parameterized molecular dynamics methods. A reasonable size is on the order of 25×25×35 Å, or about 1500 to 2000 atoms. For the Fe-oxide-water model of Rustad et al. (1995), such system sizes require about 18 sec/timestep on a single 500 MHz pentium III processor (note that this model is more computationally demanding than simpler, nondissociating water models such as PSPC or TIP4P). The methods used for million-atom types of MD simulations do not help much in this regime, as it is close to the crossover in terms of computational overhead for the O(N) methods (Kutteh and Nicholas 1995). In other words, one can go to larger scales than this at relatively small cost, but the time-savings at this particular scale is minimal. Because little is known about surface structural features above this scale, there is currently no compelling reason to extend the spatial scale. Parallelism can be conveniently exploited, however, to vastly reduce computation time. Because the memory requirements are minimal, these calculations are well suited to distrubuted memory "Beowulf" type parallel computers (Sterling 1999) with relatively inexpensive nodes. On 64 500 MHz pentium III nodes, the time to execute one timestep is about 0.29 seconds, making nanosecond simulations a reasonable proposition.

Rustad et al. (unpublished) investigated the stability of the magnetite surface shown in Figure 14 in a solvated environment. The starting configuration consisted of a 20 Å layer of ice sandwiched between a 15-Å hydroxylated slab of magnetite (001). The simulation was run for about 2 nanoseconds at 300 K ion temperature on 64 500-MHz processors connected with a GIGANET network, consuming about 20 days of real time. A major effect of solvation is an extensive secondary hydroxylation of the surface, with additional protons being picked up by the octahedral $Fe^{o}OH$ and tetrahedral $Fe^{t}OH$ surface functional groups, with the concomitant creation of hydroxide ions in the solution. This amount of charge picked up is shown in Figure 15, and a breakdown of the various populations of the surface functional groups is shown in Figure 16.

The majority of the population changes take place within the first 10 picoseconds. The active surface functional groups are the singly coordinated sites. Triply coordinated surface sites have nearly constant populations throughout the simulation. This illustrates how the gas-phase calculations can be misleading. Because the gas phase proton affinities

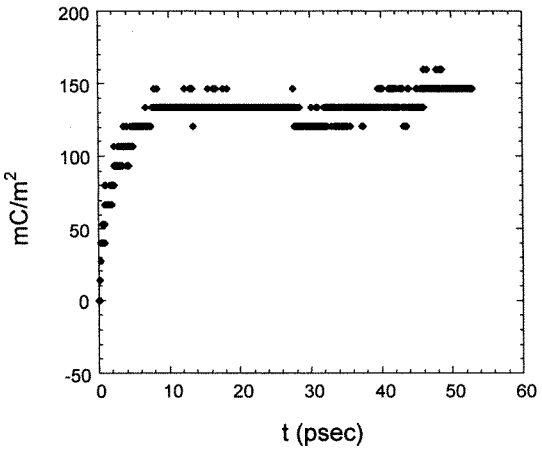

Figure 15. Accumulation of charge attendant upon solvation of the magnetite (001) surface. This charge is the result of extensive "secondary" hydroxylation of the surface.

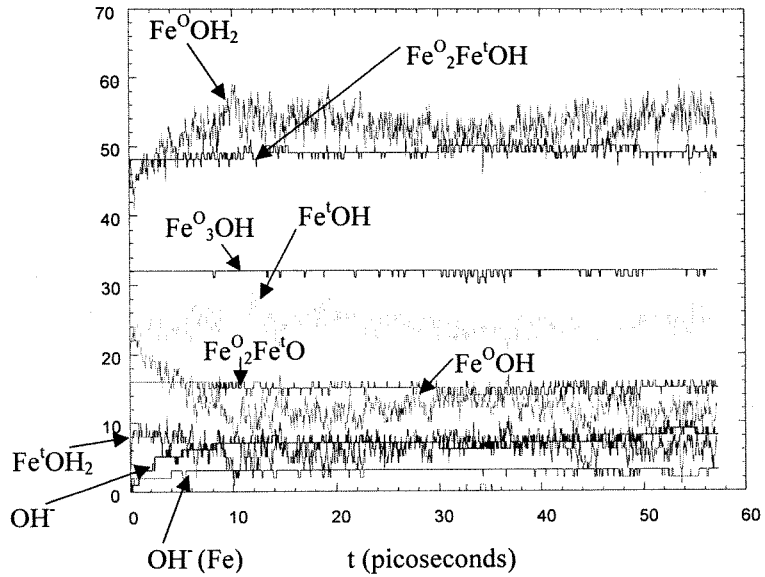

Figure 16. Evolution of the populations of various functional groups in the simulation of the solvated magnetite (001) surface. Octahedral Fe^{o}OH and tetrahedral Fe^{t}OH groups accumulate charge by acquiring protons from the solution.

of the triply coordinated sites are comparable to the other sites, one might expect them to be actively involved in proton exchange with the solution. Evidently the solvation effects make these groups relatively inert. The inertness is a result of the difficulty of solvating the more deeply buried triply coordinated surface sites. Because the solvent relaxation on deprotonation is ineffective, the sites are in fact less acidic than would have been predicted by the gas-phase proton binding energies. The sites also are much less acidic

than would be predicted by the MUSIC model. The significant number of Fe^{t}OH$_2$ sites is consistent with the gas-phase binding energies but remains in disagreement with the MUSIC predictions that nearly all the singly coordinated tetrahedral sites should be in the Fe^{t}OH state. This small simulation is meant only as an illustration of what kinds of systems are now within reach for full molecular dynamics simulations of the solvated, hydroxylated oxide surface. More work will be needed on this system to determine whether this view of the surface is viable. Numerical experiments in progress include virtual surface titrations involving the addition of acid ($HClO_4$), base (NaOH), and variations in ionic strength [$NaClO_4$]. These experiments will yield valuable insight into the structure of the electrical double layer and the effect of surface ion pairing.

REMARKS

The approach taken in the research described here is characterized by a very simple model construction phase, followed by an extensive series of tests involving information from *ab initio* electronic structure theory, mineralogy, aqueous chemistry, and high vacuum surface science. As of the time of this review, classical models are the only models simple enough to perform the necessary benchmarking calculations in all these areas and also are the only models that can be extended to 10,000 atom/nanosecond timescale simulations of interfacial phenomena.

Molecular modeling methods comprise the only reasonable theoretical framework for connecting this diverse range of experimental observations. In the future, *ab initio* methods will eclipse at least some of the range of applicability of classical simulations. At the same time, the length and time scales available to classical simulations will increase. Advances will take place in potential function formulation, allowing a greater range of phenomena to be investigated with classical simulation. There is room for employing electronic structure investigations to arrive at a better representation of the fundamental physics of the chemical bond (Parr and Pearson 1983; Gibbs et al. 1998) and to use this information to construct more accurate and flexible potential functions. A recent example is the development of potential functions capable of describing the oxidation of aluminum (Cambpell et al. 1999) and water (Burnham et al. 1999).

The major limiting factor in large-scale simulation will be the creation of a body of experimental observation which allows posing meaningful molecular level problems at scales of 10 to 1000 nm. Some chemical problems at these scales are already being addressed experimentally (Weidler et al. 1998a,b; Banfield et al. 2000). If it turns out that there are important influences of nano-mesoscale structure on chemical reactivity in geochemistry, simulation will play a large role in sorting out the factors responsible for these nanoscale structure-function relationships. Such factors might involve fluid dynamics and mixing at the interface, the influence of crystal surface roughness on intrinsic reactivity and on the surface potential, and chemomechanical effects such as stress-induced dissolution (Scudiero et al. 1999).

ACKNOWLEDGMENTS

This work, along with the bulk of the research described herein, was supported by the U.S. Department of Energy, Office of Basic Energy Sciences, Engineering and Geosciences Division, Contract 18328. The author is grateful to Nick Woodward in particular for his program management support from this office, which included funds for the purchase of the 96-node "pile of PCs" used for the computationally intensive parts of this research. Discussions and input from Eric Bylaska, Scott Chambers, Dave Dixon, Andy Felmy, Mike Henderson, Steve Joyce, Chuck Peden, Kevin Rosso, Theva

Thevuthasan, and Evgeny Wasserman of Pacific Northwest National Laboratory were essential. Many of their ideas have been instrumental in forming the basis for the research reviewed here. The National Energy Research Supercomputing Center is acknowledged for a generous grant of computer time. Scott Jackson and Ryan Braby are acknowledged for their help in keeping the "pile of PCs" functioning. The author is very grateful for technical reviews by Jim Kubicki and two anonymous reviewers and to Andrea Currie and Jamie Benward for editorial assistance. Pacific Northwest National Laboratory is operated for the U.S. Department of Energy by Battelle Memorial Institute under Contract DE-AC06-76RL01830.

REFERENCES

Akesson R, Pettersson LGM, Sandstrom M, Wahlgren U (1994) Ligand field effects in the hydrated divalent and trivalent metal ions of the first and second transition periods. J Am Chem Soc, 116:8691-8704

Allen MP, Tildesley DJ (1989) Computer Simulation of Liquids. Oxford University Press

Banfield JF, Welch SA, Zhang HZ, Ebert TT, Penn RL (2000) Aggregation-based crystal growth and microstructure development in natural iron oxyhydroxide biomineralization products. Science 289:751-754

Beattie JK, Best SP, Skelton BW, White AH (1981) Structural studies on the cesium alums, $CsM(III)[SO_4]_2 12H_2O$. J Chem Soc - Dalt Tran 10:2105-2111

Bebie J, Schoonen MAA, Strongin DR, Fuhrmann M (1998) Surface charge development on transition-metal sulphides: An electrokinetic study. Geochim Cosmochim Acta 62:633-642

Bennett CH (1975) Exact defect calculations in model substances. *In*: Diffusion in Solids: Recent Developments. Nowick AS, Buron JJ (eds), p 73

Blesa, MA, Weisz AD, Morando PJ, Salfity JA, Magaz GE, Regazzoni AE (2000) The interaction of metal oxide surfaces with complexing agents dissolved in water. Coord Chem Rev 196:31-63

Blonski S, Garofalini SH (1993) Molecular dynamics simulations of α-alumina and γ-alumina surfaces. Sur Sci 295:263-274

Bloechl PE (1994) Projector augmented wave method. Phys Rev B - Cond Mat 50:17953-17979

Brown GE, Henrich VE, Casey WH, Clark DL, Eggleston C, Felmy AR, Goodman DW, Gratzel M, Maciel G, McCarthy MI, Nealson KH, Sverjensky DA, Toney MF, Zachara JM (1999) Metal oxide surfaces and their interactions with aqueous solutions and microbial organisms. Chem Rev 99:77-174

Brown GE Jr., Chambers SA, Amonette JE, Rustad JR, Kendelewicz T, Liu P, Doyle CS, Grolimund D, Foster-Mills NS, Joyce SA, Thevuthasan T (2000) Interaction of aqueous chromium ions with iron oxide surfaces, ACS EMSP Symposium Proceedings, in press

Burnham CJ, Li JC, Xantheas SS, Leslie M (1999) The parametrization of a Thole-type all-atom polarizable water model from first principles and its application to the study of water clusters (n=2-21) and the phonon spectrum of ice. IH J Chem Phys 110:4566-4581

Campbell T, Kalia RK, Nakano A, Vashishta P, Ogata S, Rodgers S (1999) Dynamics of oxidation of aluminum nanoclusters using variable charge molecular-dynamics simulations on parallel computers. Phys Rev Let 82:4866-4869

Car R, Parrinello M (1985) Unified approach for molecular dynamics and density functional theory. Phys Rev Let 55:2471-2474

Chambers SA, Thevuthasan S, Joyce SA (2000) Surface structure of MBE-grown $Fe_3O_4(001)$ by X-ray photoelectron diffraction and scanning tunneling microscopy. Surf Sci Let 450:L273-L279

Charlton G, Howes PB, Nicklin CL, Steadman P, Taylor JSG, Muryn CA, Harte SP, Mercer J, McGrath R, Norman D, Turner TS, Thornton G (1997) Relaxation of $TiO_2(110)$-(1×1) using surface X-ray diffraction. Phys Rev Let 78:495-498

Corrales LR (1999) Dissociative model of water clusters. J Chemical Physics 110:9071-9080

Curtiss LA, Halley JW, Hautman J, Rahman A (1987) Nonadditivity of ab-initio pair potentials for molecular dynamics of multivalent transition metal ions in water. J Chem Phys 86:2319-2327

de Leeuw NH, Parker SC, Catlow CRA, Price GD (2000) Proton-containing defects at forsterite (010) tilt grain boundaries and stepped surfaces. Am Min 85:1143-1154

de Leeuw NH, Parker SC (1998) Surface structure and morphology of calcium carbonate polymorphs calcite, aragonite, and vaterite: An atomistic approach. J Phys Chem B 102:2914-2922

de Leeuw NH, Watson GW, Parker SC (1996) Atomistic simulation of adsorption of water on three-, four- and five-coordinated surface sites of magnesium oxide. J Chem Soc-Far Trans 92:2081-2091

Dzwinel W, Yuen DA (2000) A two-level, discrete-particle approach for simulating ordered colloidal structures. J Col Int Sci 225:179-190

Eggleston CM, Stumm W (1993) Scanning tunneling microscopy of Cr(III) chemisorbed on α-Fe_2O_3 (001) surfaces from aqueous solution: Direct observation of surface mobility and clustering. Geochim Cosmochim Acta 57:4843-4850

Felmy AR, Rustad JR (1998) Molecular statics calculations of proton binding to goethite surfaces: Thermodynamic modeling of the surface charging and protonation of goethite in aqueous solution. Geochim Cosmochim Acta 62:25-31

Ferris KF (1992) SCF and correlated level determination of the molecular and vibrational structure of orthosilicic acid, $Si(OH)_4$. THEOCHEM-J Mol Struc 89:499-506

Fenter P, Cheng L, Rihs S, Machesky M, Bedzyk MJ, Sturchio NC (2000) Electrical double-layer structure at the rutile-water interface as observed *in situ* with small-period X-ray standing waves. J Col Int Sci 225:154-165

Frenkel D, Smit B, Eds. (1996) Understanding Molecular Simulation: From Algorithms to Applications, 443 p. Academic Press, New York

Gibbs GV, Hill FC, Boisen MB, Downs RT (1998) Power law relationships between bond length, bond strength and electron density distributions. Phys Chem Min 25:585-590

Gibson AS, Lafemina JP (1997) Structure of Mineral Surfaces *In:* Physics and Chemistry of Mineral Surfaces. PV Brady (ed) p 1-62

Giordano L, Goniakowski J, Suzanne J (1998) Partial dissociation of water molecules in the (3×2) water monolayer deposited on the MgO (100) surface. Phys Rev Let 81:1271-1273

Guenard P, Renaud G, Barbier A, Gautier-Soyer M (1998) Determination of the alpha-Al_2O_3(0001) surface relaxation and termination by measurements of crystal truncation rods. Surf Rev Let 5:321-324

Halley JW, Rustad JR, Rahman A (1993) A polarizable, dissociating molecular dynamics model for liquid water. J Chem Phys 98:4110-4119

Halley JW, Smith BB, Walbran S, Curtiss LA, Rigney RO, Sutjianto A, Hung NC, Yonco RM, Nagy Z (1999) Theory and experiment on the cuprous-cupric electron transfer rate at copper electrode. J Chem Phys 110:6538-6552

Harding JH (1997) Mesoscopic modeling. Current Opinion in Solid State & Materials Science, 2:728-732

Hartzell CJ, Cygan RT, Nagy KL (1998) Molecular modeling of the tributyl phosphate complex of europium nitrate in the clay hectorite. J Phys Chem A 102:6722-6729

Hass KC, Schneider WF, Curioni A, Andreoni W (2000) First-principles molecular dynamics simulations of H_2O on α-Al_2O_3 (0001). J Phys Chem B 104:5527-5540

Henderson MA, Joyce SA, Rustad JR (1998) Interaction of water with the (1×1) and (2×1) surfaces of α-Fe_2O_3(012). Surf Sci 417:66-82

Hess AC, McMillan PF, Okeeffe M (1988) Torsional barriers and force-fields in H_4TO_4 molecules and molecular-ions (T=C, B, AL, SI). J Phys Chem 92:1785-1791

Hiemstra T, VanRiemsdijk WH, Bolt GH (1989) Multisite proton adsorption modeling at the solid/solution interface of (hydr)oxides: A new approach. I Model description and evaluation of intrinsic reaction constants. J Col Inter Sci 133:91-104

Hiemstra T, Venema P, VanRiemsdijk WH (1996) Intrinsic proton affinity of reactive surface groups of metal (hydr)oxides: The bond valence principle. . J Col Inter Sci, 184:680-692

Ilton ES, Veblen DR, Moses CO, Raeburn SP (1997) The catalytic effect of sodium and lithium ions on coupled sorption-reduction of chromate at the biotite edge-fluid interface. Geochim Cosmochim Acta 61:3543-3563

Jones F, Rohl AL, Farrow JB, van Bronswijk W (2000) Molecular modeling of water adsorption on hematite. Phys Chem Chemical Physics 14:3209-3216

Kim YJ, Gao Y, Chambers SA (1997) Selective growth and characterization of pure, epitaxial α-$Fe_2O_3(0001)$ and $Fe_3O_4(001)$ films by plasma-assisted molecular beam epitaxy. Surf Sci 371:358-370

Kutteh R, Nicholas JB (1995) Implementing the cell multipole method for dipolar and charged dipolar systems. Comp Phys Com 86:236-254

Laberty C, Navrotsky A (1998) Energetics of stable and metastable low-temperature iron oxides and oxyhydroxides. Geochim Cosmochim Acta 62:2905-2913

Langel W, Parrinello M (1994) Hydrolysis at stepped MgO surfaces. Phys Rev Let 73:504-507

Lindan PJD, Harrison NM, Holender JM, Gillan MJ (1996) First-principles molecular dynamics simulation of water dissociation on TiO_2 (110). Chem Phys Let 261:246-252

Liu P, Kendelewicz T, Brown GEB Jr., Nelson EJ, Chambers SA (1998) Reaction of water vapor with α-$Al_2O_3(0001)$ and α-$Fe_2O_3(0001)$ surfaces: Synchrotron X-ray photoemission studies and thermodynamic calculations. Surf Sci 417:53-65

Martin RL, Hay PJ, Pratt LR (1998) Hydrolysis of ferric ion in water and conformational equilibrium. J Phys Chem A 102:3565-3573

Masel RI (1996) Principles of Adsorption and Reaction on Solid Surfaces. John Wiley and Sons, New York
Manceau A, Drits VA, Lanson B, Chateigner D, Wu J, Huo D, Gates WP, Stucki JW (2000) Oxidation-reduction mechanism of iron in dioctahedral smectites: II Crystal chemistry of reduced Garfield nontronite. Am Min 85:153-172
McCarthy MI, Schenter GK, Scamehorn CA, Nicholas JB (1996) Structure and dynamics of the water/MgO interface. J Phys Chem 100:16989-16995
McCoy JM, LaFemina JP (1997) Kinetic Monte Carlo investigation of pit formation at the $CaCO_3$(1014) surface-water interface. Surf Sci 373:288-299
McHale JM, Auroux A, Perrotta AJ, Navrotsky A (1997) Surface energies and thermodynamic phase stability in nanocrystalline aluminas. Sci 277:788-791
Nelson CE, Elam JW, Cameron MA, Tolbert MA, George SM (1998) Desorption of H_2O from a hydroxylated single-crystal α-Al_2O_3(0001) surface. Surf Sci 416:341-353
Nooney MG, Murrell TS, Corneille JS, Rusert EI, Hossner LR, Goodman DW (1996) A spectroscopic investigation of phosphate adsorption onto iron oxides. J Vac Sci Tech A-Vac Surf Films 14:1357-1361
Parks GA (1965) Isoelectric points of solid oxides, solid hydroxides, and aqueous hydroxo complex systems. Chem Rev 65:177-198
Parks GA, deBruyn PL (1962) The zero point of charge of oxides. J Phys Chem-US 66:967-973
Parr RG, Pearson RG (1983) Absolute hardness – Companion parameter to absolute electronegativity. J Am Chem Soc 105:7512-7516
Peden CHF, Herman GS, Ismagilov IZ, Kay BD, Henderson MA, Kim YJ, Chambers SA (1999) Model catalyst studies with single crystals and epitaxial thin oxide films. Cat Today 51:513-519
Peterson KA, Xantheas SS, Dixon DA, Dunning THJ (1998) Predicting the proton affinities of H_2O and NH_3. J Phys Chem A 102 2449-2454
Peterson ML, White AF, Brown GEB Jr., Parks G (1997) Surface passivation of magnetite by reaction with aqueous Cr(VI): XAFS and TEM results. Env Sci & Tech 31:1573-1576
Rosso KM, Rustad JR (2001) The structures and energies of AlOOH and FeOOH polymorphs from plane wave pseudopotential calculations. Am Min, in press
Rustad JR, Dixon DA (2001) Computational studies of mineral-water interfaces. *In:* Molecular Modeling of Clay Minerals. Kubicki JD, Bleam WF (eds) Clay Mineral Society Washington, DC, in press
Rustad JR, Dixon DA, Felmy AR (2000b) Intrinsic acidity of aluminum, chromium (III) and iron (III) μ_3-hydroxo functional groups from *ab initio* electronic structure calculations. Geochim Cosmochim Acta 64:1675
Rustad JR, Dixon DA, Kubicki JD, Felmy AR (2000a). The gas phase acidities of tetrahedral oxyacids from *ab initio* electronic structure theory. J Phys Chem A 104:4051-4057
Rustad JR, Dixon DA, Rosso KM, Felmy AR (1999a) Trivalent ion hydrolysis reactions: A linear free energy relationship based on density functional electronic structure calculations. J Am Chem Soc 121:3234-3235
Rustad JR, Felmy AR (2000d) Molecular statics calculations of acid/base reactions on magnetite (001). *In:* Interfacial Processes: Theory and Experiment. Halley JW (ed), American Chemical Society Proceedings, in press
Rustad JR, Felmy AR, Hay BP (1996a) Molecular statics calculations for iron oxide and oxyhydroxide minerals: Toward a flexible model of the reactive mineral-water interface. Geochim Cosmochim Acta 60:1553-1562
Rustad JR, Felmy AR, Hay BP (1996b) Molecular statics calculation of proton binding to goethite surfaces: A new approach to estimation of stability constants for multisite surface complexation models. Geochim Cosmochim Acta 60:1563-1576
Rustad JR, Hay BP (1995) A molecular-dynamics study of solvated orthosilicic acid and orthosilicate anion using parameterized potentials. . Geochim Cosmochim Acta 59:1251-1257
Rustad JR, Hay BP, Halley JW (1995) Molecular dynamics simulation of iron(III) and its hydrolysis products in aqueous solution. J Chem Phys 102:427-431
Rustad JR, Wasserman E, Felmy AR (1999b) Molecular modeling of the surface charging of hematite - II Optimal proton distribution and simulation of surface charge versus pH relationships. Surf Sci 424:28-35
Rustad JR, Wasserman E, Felmy AR (1999c) A molecular dynamics investigation of surface reconstruction on magnetite (001). Surf Sci 432:L583-L588
Rustad JR, Wasserman E, Felmy AR (2000c) The magnetite (001) surface: Insights from molecular dynamics calculations. *In:* Properties of Complex Inorganic Solids, Volume II. Meike A, Gonis A, Turchi PEA, Rajan K (eds), Kluwer Academic/Plenum Publishers, Dordrecht, The Netherlands p 499-509

Ryan MP, Toney MF, Oblonsky LJ, Davenport AJ (2000) An x-ray diffraction study of the passive oxide film on iron. *In:* Interfacial Processes: Theory and Experiment. Halley JW (ed), American Chemical Society Proceedings, in press
Scudiero L, Langford SC, Dickinson JT (1999) Scanning force microscope observations of corrosive wear on single-crystal brushite ($CaHPO_4 . 2H_2O$) in aqueous solution. Tribology Let 6:41-55
Shapovalov V, Truong TN (2000) Ab initio study of water adsorption on α-Al_2O_3 (0001) crystal surface. The J Phys Chem B 104:9859-9863
Soper AK, Phillips MG (1986) A new determination of the structure of water at 25°C. Chem Phys 107:47-60
Sposito G (1999) On points of zero charge. Env Sci Tech 33:208-208
Stanka BI, Hebenstreit W, Diebold U, Chambers SA (2000) Surface reconstruction of Fe_3O_4(001). Surf Sci 448:49-63
Stirniman MJ, Huang C, Smith RS, Joyce SA, Kay BD (1996) The adsorption and desorption of water on single crystal MgO(100): The role of surface defects. J Chem Phys 105:1295-1298
Sterling TL, Salmon J, Becker DJ, Savarese DF (1999) How to Build a Beowulf: A Guide to the Implementation and Application of PC Clusters, MIT Press, Cambridge, Massachusetts.
Stillinger FH, David CW (1980) Study of the water octamer using the polarization model of molecular interactions. J Chem Phys 73:3384-3389
Straus JB, Voth GA (1993) A computer simulation study of free energy curves in heterogeneous electron transfer. J Phys Chem 97:7388-7391
Sturchio NC, Chiarello RP, Cheng LW, Lyman PF, Bedzyk MJ, Qian YL, You HD, Yee D, Geissbuhler P, Sorensen LB, Liang Y, Baer DR (1997) Lead adsorption at the calcite-water interface: Synchrotron X-ray standing wave and X-ray reflectivity studies. Geochim Cosmochim Acta 61:251-263
Sverjensky DA (1994) Zero point-of-charge prediction from crystal chemistry and solvation theory. Geochim Cosmochim Acta 58:3123-3129
Sverjensky DA, Sahai N (1996) Theoretical prediction of single-site surface protonation equilibrium constants for oxides and silicates in water. Geochim Cosmochim Acta 60:3773-3797
Tasker PW (1979) Stability of ionic crystal surfaces. J Physics C: Solid State Physics 12:4977-4984
Toukan K, Rahman A (1985) Molecular-dynamics study of atomic motions in water. Phys Rev B- Con Mat 31:2643-2648
Thevuthasan S, Kim YJ, Yi SI, Chambers SA, Morais, J, Denecke R, Fadley CS, Liu P, Kendelewicz T, Brown GE Jr. (1999) Surface structure of MBE-grown α-Fe_2O_3(0001) by intermediate-energy X-ray photoelectron diffraction. Surf Sci 425:276-286
Vaidehi N, Goddard WA (2000) Domain motions in phosphoglycerate kinase using hierarchical NEIMO molecular dynamics simulations. J Physl Chem A 104:2375-2383
Vanderbilt D (1990) Soft self-consistent pseudopotentials in a generalized eigenvalue formalism. Phys Rev B - Con Mat 41:7892-7895
Voogt FC (1998) NO_2-assisted molecular beam epitaxy of iron oxide films. PHD Thesis, Rijkuniversiteit Gronigent, Groningen, The Netherlands
Yoon RH, Salman T, Donnay G (1979) Predicting the point of zero charge of oxides. J Col Int Sci 70:483-493
Yuen DA, Rustad JR (1998) Workshop on computational studies of interfacial phenomena: Nanoscale to mesoscale. Electronic Geosciences, 3:supplement 1
Wang X-G, Weiss W, Shaikhutdinov SK, Ritter M, Petersen M, Wagner F, Schlogl R, Scheffler M (1998) The hematite (α-Fe_2O_3) (0001) surface: Evidence for domains of distinct chemistry. Phys Rev Let 81:1038-1041
Wasserman E, Rustad JR, Felmy AR, Hay BP, Halley JW (1997) Ewald methods for polarizable surfaces with application to hydroxylation and hydrogen bonding on the (012) and (001) surfaces of α-Fe_2O_3. Surf Sci 385:217-239
Wasserman E, Rustad JR, Felmy AR (1999) Molecular modeling of the surface charging of hematite - I. The calculation of proton affinities and acidities on a surface. Surf Sci 424:17-19
Watanabe H, Seto J (1990) The intrinsic equilibrium constants of the surface hydroxyl groups of maghemite and hematite. Bul Chem Soc Jap 63:2916-2921
Weidler PG, Hug SJ, Wetche TP, Hiemstra T (1998a) Determination of growth rates of (100) and (110) faces of synthetic goethite by scanning force microscopy. Geochim Cosmochim Acta 62:3407-3412
Weidler PG, Degovics G, Laggner P (1998b) Surface roughness created by acidic dissolution of synthetic goethite monitored with SAXS and N_2 adsorption isotherms. J Col Int Sci 197:1-8
Wiesendanger R, Shvets IV, Coey JMD (1994) Wigner glass on the magnetite (001) surface observed by scanning-tunneling microscopy with a ferromagnetic tip. J Vac Sci Tech B 12:2118-2121
Zhang HZ, Penn RL, Hamers RJ, Banfield JF (1999) Enhanced adsorption of molecules on surfaces of nanocrystalline particles. J Phys Chem B 103:4656-4662